Dynamic Cell Imaging: application to the diatom Phaeodactylum tricornutum under environmental stresses

Houda Bey, Florent Charton, Helena Cruz de Carvalho, Shun Liu, Richard G Dorrell, Chris Bowler, Claude Boccara, Martine Boccara

Dynamic Cell Imaging: application to the diatom Phaeodactylum tricornutum under environmental stresses

Houda Bey, Florent Charton, Helena Cruz de Carvalho, Shun Liu, Richard G Dorrell, Chris Bowler, Claude Boccara, Martine Boccara

Dynamic Cell Imaging: application to the diatom *Phaeodactylum tricornutum* under environmental stresses

Houda Bey[a], Florent Charton[b], Helena Cruz de Carvalho[b,c], Shun Liu[b], Richard G. Dorrell[b], Chris Bowler[b], Claude Boccara[a] and Martine Boccara[a,b]

[a]Institut Langevin, ESPCI Paris, PSL Research University, CNRS UMR 7587, 1 rue Jussieu, 75005 Paris, France; [b]Ecole Normale Supérieure, PSL Research University, Institut de Biologie de l'Ecole Normale Supérieure (IBENS), CNRS UMR 8197, INSERM U1024, 46 rue d'Ulm, F-75005 Paris, France; [c]Université Paris Est-Créteil (UPEC), Faculté des Sciences et Technologie, 61, avenue du Général De Gaulle, 94000 Créteil, France

ABSTRACT

The dynamic movement of cell organelles is an important and poorly understood component of cellular organization and metabolism. In this work we present a non-invasive non-destructive method (Dynamic Cell Imaging, DCI) based on light scattering and interferometry to monitor dynamic events within photosynthetic cells using the diatom *Phaeodactylum tricornutum* as a model system. For this monitoring we acquire for a few seconds movies of the signals that are related to the motion of dynamic structures within the cell (denoted scatterers), followed by a statistical analysis of each pixel time series. Illuminating *P. tricornutum* with LEDs of different wavelengths associated with short pulsed or continuous-wave modes of illumination revealed that dynamic movements depend on chloroplast activity, in agreement with the reduction in the number of pixels with dynamic behaviour after addition of photosystem II inhibitors. We studied *P. tricornutum* under two environmentally relevant stresses, iron and phosphate deficiency. The major dynamic sites were located within lipid droplets and chloroplast envelope membranes. By comparing standard deviation and cumulative sum analyses of the time series, we showed that within the droplets two types of scatterer movement could be observed: random motion (Brownian type) but also anomalous movements corresponding to a drift which may relate to molecular fluxes within a cell. The method appears to be valuable for studying the effects of various environments on microalgae in the laboratory as well as in natural aquatic environments.

HIGHLIGHTS

- Light scattering is an alternative to fluorescence to rapidly evidence dynamic processes.
- Lipid droplets are the major metabolic active sites under stress.
- A non-destructive visualization method suitable for laboratory microalgae and aquatic samples.

ARTICLE HISTORY Received 8 November 2021; Revised 14 February 2022; Accepted 17 April 2022

KEYWORDS Chloroplast; endoplasmic reticulum; iron limitation; light scattering; lipid droplets; organelle movement; phosphate limitation

Introduction

Diatoms are a diverse group of photosynthetic microorganisms which account for up to 40% of ocean primary production (Bowler *et al.*, 2010). They are distributed worldwide, from tropical and subtropical regions to polar ecosystems in oceans and fresh waters, and thus have an exceptional ability to adapt to highly dynamic aquatic environments (Falciatore *et al.*, 2020; Pierella Karlusich *et al.*, 2020). These include stressful environmental fluctuations and chronic scarcities of key nutrients including nitrogen, phosphorus and iron (Abida *et al.*, 2015; Alipanah *et al.*, 2015; Cruz de Carvalho *et al.*, 2016; Kazamia *et al.*, 2018; Gao *et al.*, 2021), extreme temperatures ranging from continuously near-freezing in ocean polar regions to hot currents in equatorial oceans (Yao *et al.*, 2012; Liang *et al.*, 2019) or highlight illumination levels (Domingues *et al.*, 2012; Alboresi *et al.*, 2016).

Diatoms have a complex evolutionary origin, which involved a secondary symbiotic event where a heterotrophic eukaryote engulfed a microalga of the red lineage (Cavalier-Smith, 1999). This has led to the presence of four membranes around the plastids of diatoms, with the outermost chloroplast membrane joined to the endoplasmic reticulum (ER) and several internal chloroplast compartments including the periplastid compartment (located between the second and third innermost membranes). To identify the metabolically active organelles in diatom cells under stress, methods involving organelle isolation, biochemical methods, genomic, and cell products characterization have been very valuable (Abida *et al.*, 2015; Lupette *et al.*, 2019). Fluorescence imaging techniques with high spatial and temporal resolution have previously been used to further investigate dynamic processes in stressed diatoms (Lupette *et al.*, 2019; Jaussaud *et al.*, 2020). Indeed, cytological methods involving the use of specific stains or of fluorescent proteins are widely used in microscopy. Green Fluorescent Protein (GFP) tagged proteins are used to visualize and track in real time proteins of interest as well as cell organelles (Apt *et al.*, 2002; Kazamia *et al.*, 2018).

CONTACT Claude Boccara claude.boccara@espci.fr; Martine Boccara mboccara@bio.ens.psl.eu

Among many GFP applications, Fluorescence Recovery After Photobleaching (FRAP) has been used to characterize the transport of integral membrane proteins from the endoplasmic reticulum to lipid droplets in yeast (Jacquier *et al.*, 2011).

Studies of biological materials by Dynamic Cell Imaging (DCI), also called Dynamic Full field Optical Transmission Tomography (D-FFOTT), are based on the detection of light back-scattered by movements of subcellular organelles (denoted scatterers) and do not need elaborate molecular manipulations, unlike GFP. This method is non-invasive and non-destructive (Apelian *et al.*, 2016; Thouvenin *et al.*, 2017*a*, 2017*b*; Scholler *et al.*, 2019). A more recent variation of DCI, working in transmission and forward scattering, that we use here is described in Thouvenin *et al.* (2021). DCI was shown to be associated with metabolic activity as it disappeared when cells were fixed or treated with the metabolic inhibitor deoxy-glucose (Apelian *et al.*, 2016). DCI appeared to be a promising technique for studying cell substructural dynamics in eukaryotic microorganisms that cannot be genetically modified. Thus we first studied the model unicellular photosynthetic microorganism *Phaeodactylum tricornutum* in responding to nutrient stress conditions.

We studied two major nutrient stresses: iron and phosphate depletion. Iron (Fe) is an essential micronutrient for all living cells since it is crucial for photosynthesis and respiration, and for phytoplankton it is a cofactor of proteins involved in a number of metabolic reactions. Iron deficiency leads to a decrease in photosynthetic efficiency (Kolber *et al.*, 1994) by inducing partial blocking of the electron transfer between photosystem II (PSII) and photosystem I (PSI) (Roncel *et al.*, 2016). Iron is an important growth-limiting or co-limiting nutrient in many regions of the world's ocean in which diatoms are important primary producers (Ustick *et al.*, 2021).

Phosphate is a fundamental element of all living cells as it is a constituent of membranes, nucleic acids and other biomolecules. Phosphate limitation and co-limitation are frequently observed in low northern latitudes (Ustick *et al.*, 2021). Deficiency of its inorganic form (Pi) is a common form of stress that strongly limits ocean primary production. Indeed, inorganic phosphate (Pi) deficiency is known to induce a shift in diatom metabolism leading to arrested cell growth and production of lipid vesicles (Cruz de Carvalho *et al.*, 2016). It has recently been shown that these lipid vesicles (also known as lipid bodies or lipid droplets) accumulate in the vicinity of the chloroplasts (Alipanah *et al.*, 2018; Lupette *et al.*, 2019). Indeed limitation of nutrients such as nitrate and phosphate leads to remodelling of cellular membranes, with degradation of membrane phospholipids and fatty acids which are redirected to lipid bodies (Goss *et al.*, 2020).

Various possible kinds of organellar movements can be observed in cells from a pure Brownian type to drifting at a defined velocity (Saunter *et al.*, 2009). Here we characterize the small amplitude movements of scatterers within *P. tricornutum* by analysing the time series associated with each pixel of the field of view in order to get a map of the transmission, the standard deviation, the cumulative sum and the average frequency. Through this computational analysis, we were able to highlight random and non-random movements suggesting that this method can spot *in vivo* molecular fluxes.

Materials and methods

Diatom culture conditions

Phaeodactylum tricornutum CCMP632 was cultured in artificial seawater (40 g l^{-1}, Sigma) supplemented with f/2 nutrients and vitamins (F/2 Media Kit, Bigelow National Center for Marine Algae and Microbiota, USA) under continuous shaking (100 rpm) at 19°C under cool white fluorescent lights (30 µmol m^{-2} s^{-1}) with a 12 h photoperiod. For phosphate depletion studies equal aliquots of 4-day-old cultures from the same batch culture were inoculated in parallel in fresh f/2 media (control conditions) and in 250 ml fresh f/2 media without phosphate supplement (Pi depleted) and cultured in the same conditions as described above for 8 days.

For iron depletion, cultures were grown in enhanced seawater medium with or without iron-EDTA (supplemented concentration 86.9 µmol l^{-1}), and analysed after two subcultures (with starting inoculum of 100 000 cells ml^{-1}) for 8 days. All cell lines were grown in ventilator-capped plastic culture flasks (Sigma) to minimize contamination into the growth media by residual iron or phosphorus from the culture flask. Cells were collected by centrifugation and mixed with melted 1% agar (42°C) in culture medium and immediately observed after jellification (20°C).

For photosystem II inhibition, we used 3-(3,4-dichlorophenyl)- 1,1-dimethylurea (DCMU; 40 µM) and hydroxylamine (HA; 2 mM) solutions in water. Cells were incubated for 10 minutes at room temperature with inhibitors, embedded in agar and immediately observed.

DCI: Data acquisition and treatment

To follow the movement of internal structures within diatoms at the pixel level we used the

time variation of optical tomographic images, the principle of which is described in detail in Apelian *et al.* (2016), Thouvenin *et al.* (2017*a*, 2017*b*) and Scholler *et al.* (2019), but using a new experimental approach, called Dynamic Full Field Optical Transmission Tomography (D-FFOTT) that is described in detail in Thouvenin *et al.* (2021). In brief, the sample is illuminated in transmission by the incoherent light emitted by a LED; this beam is partially scattered by the sample structure and partially transmitted. Both beams propagate along the same path and interfere with a phase shift (known as the Gouy phase shift) that depends on the relative position of the scatterer and of the focus of the objective. The subcellular organelle movements induce a time variation of the signal detected on each pixel of the camera. We use a Photonfocus A1024B camera working at 140 Hz with a CMOS image sensor with a 0.2 Me^{-} full well capacity that ensures measurements with a good signal-to-noise ratio. The light source (LED + stabilized power supply) is very stable and so the main source of noise relates to photoelectron statistics associated with each camera pixel, known as 'shot noise'. In our experiment each pixel of the camera stores N = 160 000 electrons (we work below the saturation of 0.2 Me^{-}), so the expected shot noise is $\sqrt{N} = 400$, i.e. allowing the detection of a variation in transmission of 1/400 the average value.

To represent the evolution of signal over time we displayed a number of characteristic images extracted from a movie of typically 100–200 images lasting a few seconds (frequency 140 images s^{-1}), as follows: (1) The transmission image is analysed to check the stability of the cells and the lack of bleaching. (2) Steps 1 and 2 are run with the open source platform Fiji (Schindelin *et al.*, 2012). (3) The average cumulative sum of one tenth of the movie (Scholler, 2019) is compared with the standard deviation of each pixel. Unlike pure Brownian motion, a biased Brownian motion is hyper-diffusive. Organelle movements in cells are either a drift induced for instance by a flow, or a random Brownian-like motion. Often, the time series of the signals linked to the organelle movements exhibit a combination of these two movements referred to as 'biased Brownian motion'. Using the cumulative sum instead of the standard deviation is a direct way to distinguish the two types of motion. Indeed summing Brownian steps will give a trajectory that stays close to zero whereas if there is a small bias added to the Brownian random steps (Supplementary fig. S1), it will be summed for every sample and could be revealed by the cumulative sum; a more detailed description of this approach can be found in Scholler (2019). We used the cumsum function of Matlab which, when a small bias is present, is more adapted to reveal anomalous Brownian motion and, in addition, increase the signal-to-noise ratio of the DCI. The normalization used the shot noise normal distribution in the background. All experiments were repeated three times.

Fluorescence microscopy

We used GFP (green fluorescent protein) constructs to characterize the dynamic location of several *P. tricornutum* organelles, favouring previously established reporter proteins for each organelle (Liu *et al.*, 2016). C-terminal GFP constructs were assembled by Gibson assembly into pPhat vectors, and introduced into wild-type *P. tricornutum* by biolistic transformation, followed by selection on 100 μg ml^{-1} zeocin-supplemented ESAW-agar plates, as previously described (Falciatore *et al.*, 1999). The selected markers were: GFP with no targeting signal in which the signal accumulates in the cytoplasm; GFP fused to BiP (Binding immunoglobulin protein), localized in the chloroplast endoplasmic reticulum (Apt *et al.*, 2002); and GFP fused to the N-terminal extension comprising a signal peptide and a transit peptide of cpHsp70 (chloroplastic heat shock protein 70), expressed in the periplastid compartment (Gould *et al.*, 2006). Full construct vector sequences are provided in Supplementary table S1. For all GFP experiments transgenic diatoms were analysed using a standard inverted epifluorescence microscope (Nikon Ti-E) equipped with an oil immersion objective (90×, 1.4 NA) and an EMCCD camera (Andor Ixon Ultra X-10381). GFP was excited at 488 nm and the emitted fluorescence detection window was 500–550 nm. The sensitivity of the camera used for bright field recording (10 times lower full well capacity than the Photon Focus CMOS camera) did not allow merging of the two types of signal (fluorescence and interferometry) using the same field of view.

We also used multimodal imaging combining interferometry and fluorescence in a single optical setup (described in Thouvenin *et al.*, 2017*b*) to compare the fluorescent labelling with the distribution of DCI signals within lipid bodies. Diatoms were incubated with BODYPY 505/515 (dissolved in DMSO; 0.1 μg ml^{-1} final concentration) for 30 minutes and observed by DCI and fluorescence. In this system we used a LED source centred at 470 nm (M470L4, Thorlabs, Newton, NJ, USA) for the excitation and filtered with a bandpass filter centred on 475 nm with a bandwidth of 50 nm

(Semrock FF02-475/50-25). The interferometry signal was recorded on a custom camera (Quartz 2A750, Adimec). The emitted fluorescence was filtered with another bandpass filter centred on 540 nm (Semrock FF01-540/50-25) then imaged using a sCMOS camera (Hamamatsu Photonics). A dichroic mirror at 506 nm (Semrock FF506-Di03-25) separates excitation and fluorescence wavelengths. The experiment was repeated twice with similar results.

Results

DCI reveals the dynamics of diatom organelles

Diatoms grown in supplemented artificial seawater were embedded into agar in the same medium and immediately observed with the DCI set up (or D-FFOTT; Thouvenin *et al.*, 2021). The preparation was illuminated for a few seconds (pulsed light, 1 ms, LED blue 455 nm) at a few tens of Hz (140 frames s^{-1}) and a film recorded synchronously at the same frequency. We used pulsed illumination to freeze movements within cells and to avoid light saturation of photosynthesis. When observing the film of the transmission, no overall cell movement was detected and the diatoms looked still (Supplementary movie S1). When we computed the standard deviation of each pixel for all the frames of the film we observed two sites of movement within the cells: vesicles or droplets and the chloroplast membrane. The figures display the cells' metabolic activity (Apelian *et al.*, 2016); the colour map code (ImageJ, 16 colours) is such that red corresponds to the highest activity and dark blue to the lowest activity that is linked to the speed of the scatterers' movements. In the vicinity of the chloroplast, vesicles or lipid droplets of different sizes appeared green, yellow and red with the most dynamic regions located at edges of the droplet (Fig. 1., red arrow). The other highly dynamic location corresponded to the chloroplast membranes and often looked punctuated (Fig. 1., white arrows). Interestingly, these results were observed independently of the three morphotypes that were present in the cultures (fusiform, triradiate or oval) (De Martino *et al.*, 2007). *P. tricornutum* cells were also illuminated with a green LED (505 nm) or a deep red LED (735 nm, a spectral region where no *P. tricornutum* pigments absorb and no photosystems are excited). The green LED dynamic region surrounding the chloroplast and the strong signal at the edges of the vesicles were very similar to what was detected with the 455 nm LED (Fig. 2., Supplementary fig. S2A). Histogram profiles of the standard deviation of signal intensity of each pixel were very similar between blue and 505 nm LEDs with a shoulder corresponding to the strongest signals (Supplementary fig. S2B). When we used the 735 nm LED the signal was significantly reduced to one-third (Fig. 2., Supplementary figs S2A and S2B). We tested two inhibitors at concentrations inhibiting photosystem II: 3-(3,4-dichlorophenyl)-1,1-dimethylurea (DCMU; 40 µM) or hydroxylamine (HA; 2mM) and measured the number of pixels with dynamic behaviour. We observed a significant reduction to one-third in the presence of both inhibitors suggesting that the dynamic structures we described depend on chloroplast metabolic activity (Fig. 2.). To further investigate this observation, we compared image acquisition between continuously and pulsed LED lighting (Fig. 1.). No obvious dynamic structures within the cell were highlighted when illumination was continuous, unlike with pulsed light, although no difference in transmission was observed meaning that no photobleaching was involved (Fig. 1., C, B, D). The continuous illumination (1000 W m^{-2}) with the 455 nm LED corresponded to the high illumination level used to block chloroplast activity while the pulsed illumination (pulses of 0.25 ms at 140 Hz) corresponded to a low illumination level (30 W m^{-2} or 120 µmol photons m^{-2} s^{-1}). This suggested that the high continuous light photon budget prevents chloroplast function unlike the pulsed mode level of irradiation (average power 30 times lower, Fig. 1.) and is in agreement with the photon budget given by Prins *et al.* (2020). Our observations suggest that during continuous exposure to light, chloroplasts are saturated with photons, which results in the low metabolic activity recorded (Bailleul *et al.*, 2011). We reasoned that the elimination of harmful excess energy could be dissipated through heat, however using a microthermocouple immersed in the sample cuvette (volume 5 µl) we did not detect an overall measurable increase in temperature (< 0.1°C) under the same illumination level. This low temperature increase was confirmed by an estimation of the power absorbed by the algae in the sample volume which was found to be of a few thousandths of a degree Celsius.

Fluorescence studies indicate dynamic movements in the chloroplast: endoplasmic reticulum and lipid bodies

To better characterize the cell compartments in which dynamic structures are localized, C-terminal GFP fusions of proteins targeted to various compartments within *P. tricornutum* cells were observed with a fluorescent microscope (same samples analysed with DCI). GFP

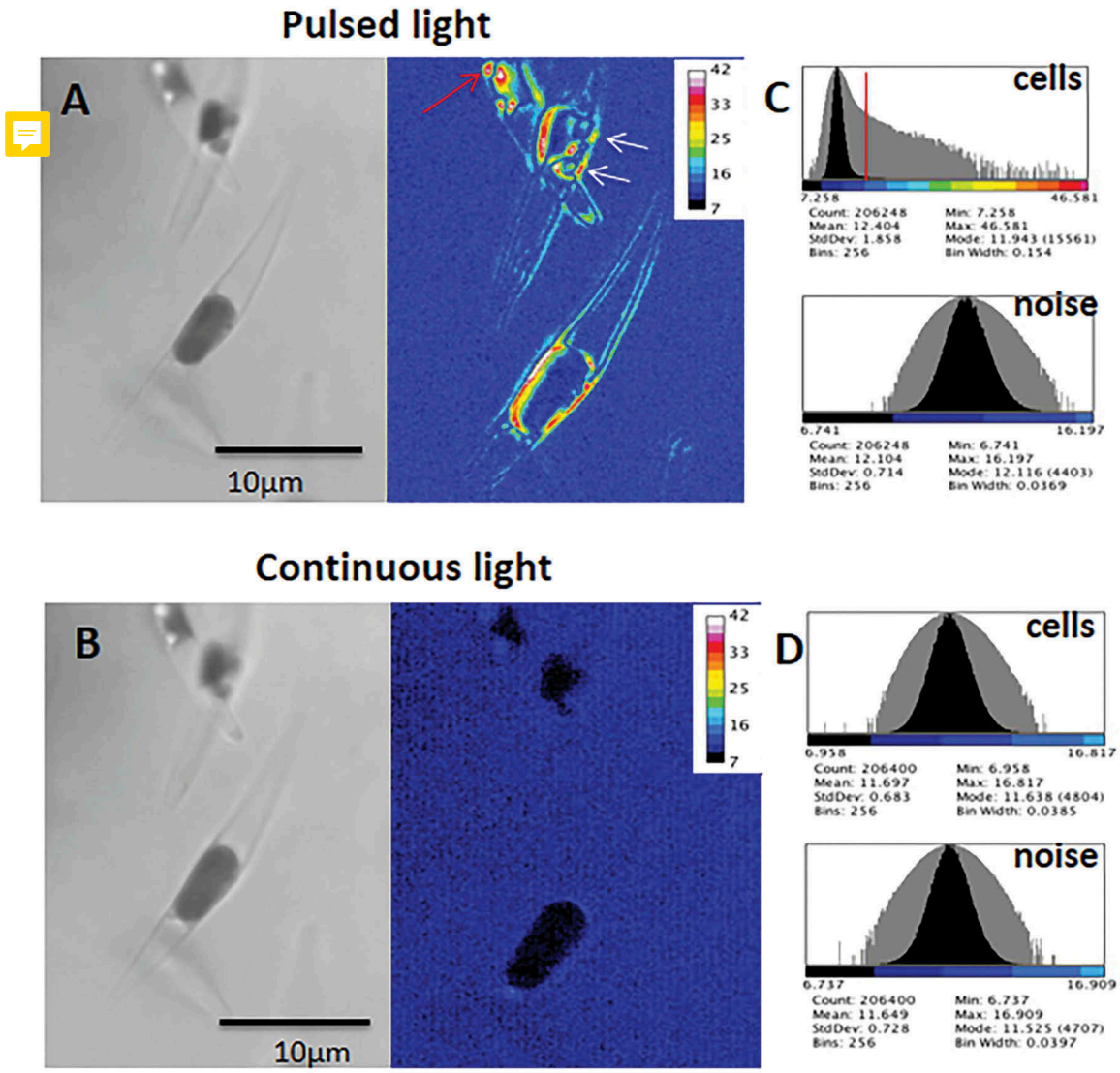

Fig. 1. Effect of continuous or pulsed lighting on intracellular movements in *Phaeodactylum tricornutum*. Cells were successively illuminated with the LED_{455}, with either continuous or pulsed light and a film recorded for a few seconds. Left image: transmission (single capture from the 100 frames movie); right image: standard deviation (scale on right) of each pixel of the same field over the 100 frames and in successive acquisition (pulsed light followed by continuous lighting). **A**: pulsed lighting; red arrow indicates lipid droplet and white arrows correspond to punctuations in chloroplast membranes. **B**: continuous lighting.

with no targeting signal was localized in the cytosol (Supplementary fig. S3, CYT). GFP fused to a bipartite targeting signal (signal sequence and transit peptide) of HSP70, enabling this protein to cross the two chloroplast membranes, did not label the vesicles suggesting that they were not associated with the periplastid compartment (PPC) (Supplementary fig. S3, PPC). In contrast, the signal for the BIP protein fused with GFP, resulting in fluorescence in the endoplasmic reticulum (ER), labelled the dynamic vesicles (Supplementary fig. S3, ER). These observations suggested that vesicles, possibly lipid droplets (see below), originate from the endoplasmic reticulum as suggested by Jaussaud *et al.* (2020).

We took advantage of a setup which combined interferometry and fluorescence (Thouvenin *et al.*, 2017*b*) to compare the location of dynamic signals with those identifying lipid bodies. For this purpose, we labelled lipid bodies with BODIPY505/515 and as shown in Fig. 3. we observed co-localization of dynamic signals and lipid labelling. In addition we showed in other cells that dynamic signals were associated with more structures than the specific signal observed by fluorescence (Supplementary fig. S4).

Dynamics of organelles in diatoms grown in iron-limited conditions

Kazamia *et al.* (2018) demonstrated that iron uptake in *Phaeodactylum* under iron-limited conditions involved an endocytosis step and a delivery

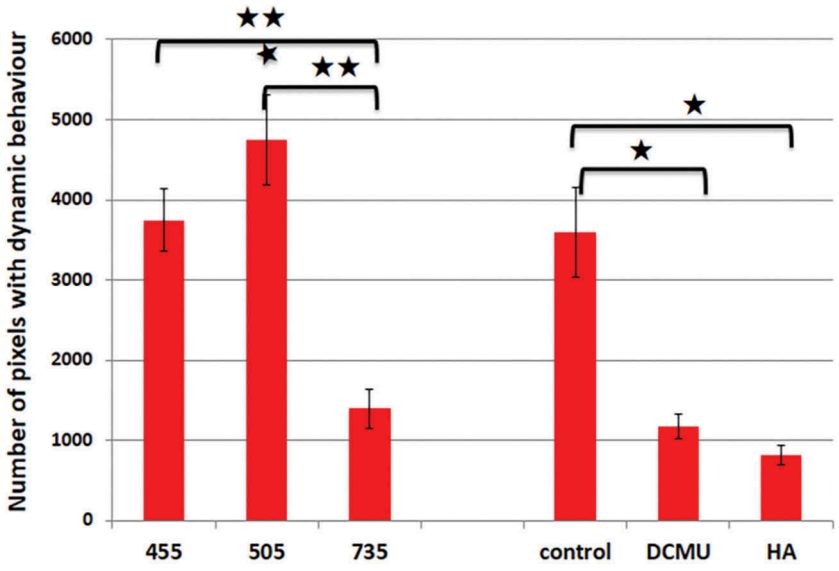

Fig. 2. Bar chart of pixels with dynamic behaviour: effects of wavelength illumination and photosystem II inhibitors. Average values plus and minus standard deviation are presented. The different wavelengths tested are: 455 nm (blue), 505 nm (green) and 735 nm (deep red). Two photosystem II inhibitors were used: DCMU (3,4-dichlorophenyl)-1,1-dimethyl-urea; 40 µM) and HA (hydroxylamine; 2 mM). 20 to 30 cells were analysed. A Wilcoxon test was carried out; the comparison of the signal observed between 455 nm (blue) and 735 nm (deep red) and between 505 nm (green) and 735 nm (deep red) gave a *p*-value of 0.0079 at a significance level of 0.05. The same test was carried out with photosystem II inhibitors: the signal observed between control and DCMU or HA gave a *p*-value of 0.03 at a significance level of 0.05.

step in the vicinity of the chloroplast. This study suggested dynamic events in *Phaeodactylum* cells when iron is limited. We thus visualized the effect of iron limitation on *P. tricornutum* intracellular dynamics after one week and two weeks of culture in iron-depleted growth media. After one week of culture in iron-depleted medium, a slight decrease in growth was observed, suggesting a growth slow-down and after two weeks a 10-fold growth reduction was observed (Table 1). Samples were analysed using DCI after one (T1) or two (T2) transfers of culture with iron-replete or iron-depleted media. In the presence of iron in the culture medium, we did not observe much difference between the two subcultures with dynamic pixels localized mostly in lipid droplets. We computed the number of pixels after removing the background noise of the same stack and found no differences between the two measurements (Table 1, Supplementary fig. S4). After one week of culture in iron-limited medium we observed a slight reduction (by about 10%) in the number of pixels with dynamic behaviour. After two weeks of culture in iron-limited medium the number of pixels with dynamic behaviour was 75% lower (Table 1, Supplementary fig. S4). The pixels with dynamic behaviour were localized in the lipid droplets, however on average there was no significant difference in the droplet diameters between iron-replete and iron-depleted conditions (1.1 ± 0.5 µm and 0.9 ± 0.2 µm respectively). All these results suggest that in the iron-depleted medium the accumulation of lipids in droplets is arrested after prolonged starvation, which may be due to the shutdown of photosynthetic carbon assimilation and/or lipid synthesis.

Dynamics of lipid bodies in diatoms subjected to phosphate deprivation

It has been previously reported that after 8 days of culture in full-nutrient media small lipid droplets start forming in *P. tricornutum* cells, suggesting a developing nutrient stress (Cruz de Carvalho *et al.*, 2016). After 8 days in full culture media we observed on average two lipid droplets per *P. tricornutum* cell and their diameters were computed (Table 2, Fig. 4., Supplementary fig. S5). The analysis of the standard deviation of signal intensity of each pixel showed that 30–50% of the droplets exhibited a dynamic behaviour (Table 2, Fig. 4., Supplementary fig. S5). In the case of *P. tricornutum* grown for 8 days in phosphate-depleted medium there was a net reduction in cell growth (2–3 times) (Cruz de Carvalho *et al.*, 2016) and a net increase in the number of droplets (5–10), which were significantly larger than when grown in Pi-replete medium (Table 2). Furthermore, the majority of the lipid droplets showed dynamic behaviour (Table 2, Fig. 4., Supplementary fig. S5). Generally, the droplets were in close association with the chloroplast but sometimes they were found

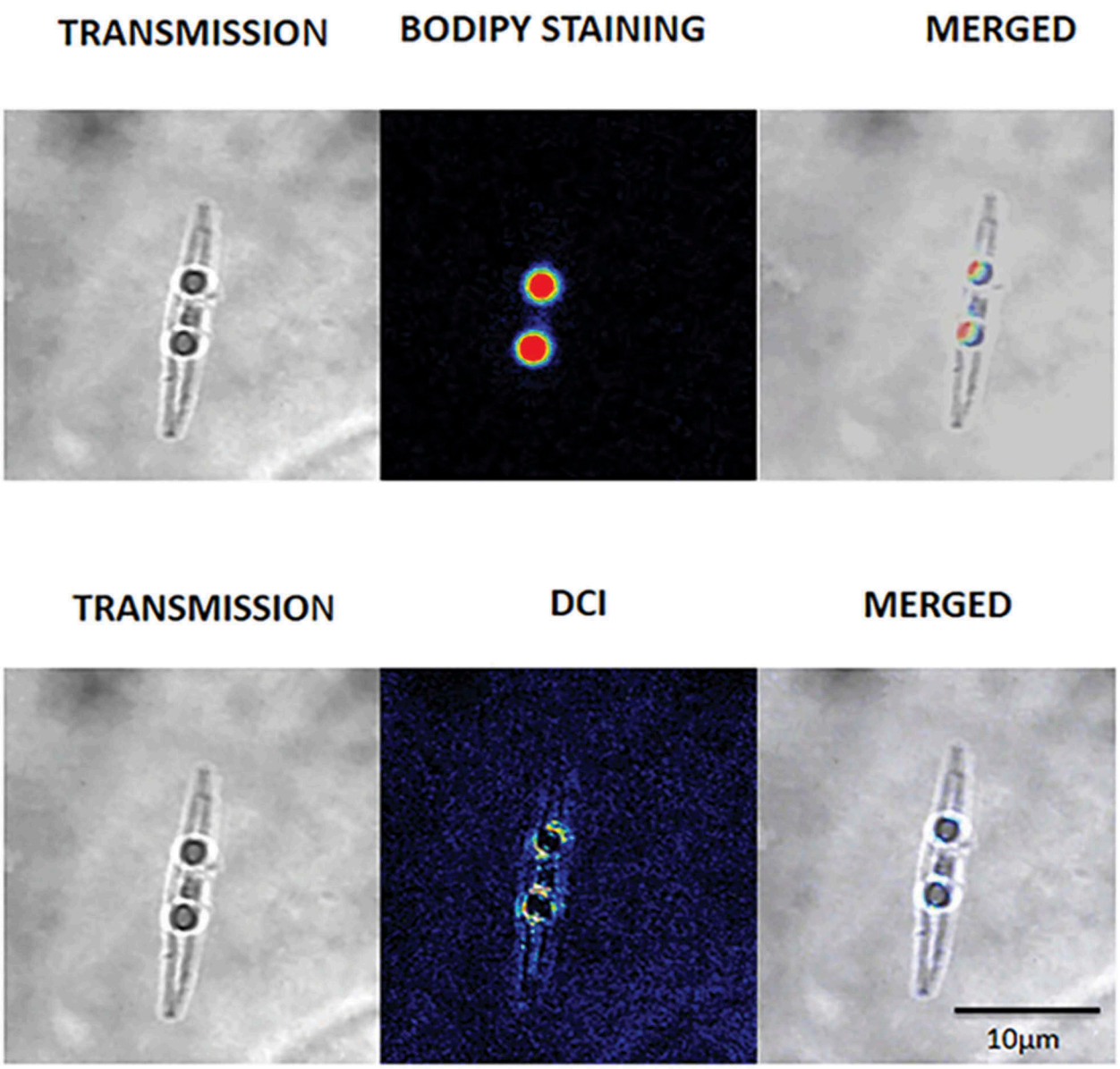

Fig. 3. Co-localization of dynamic droplets from *Phaeodactylum tricornutum* and BODIPY© labelled lipid droplets. Left panel: transmission microscopy, central panel: fluorescence (grey scale camera, green colouration), right panel merge of the two previous images. Left panel: transmission microscopy, central panel: standard deviation (grey scale camera, 16 colours), right panel merge of the two previous images. Scale bar values were deduced from the format of the image (90 × 90 µm).

Table 1. Effect of iron limitation after one (T1) and two (T2) passages on dynamic movements in *Phaeodactylum tricornutum*

	Number of cells $\times 10^6$ ml^{-1} ± SD	Average number of pixels with dynamic behaviour ± SD[a]	Number of analysed cells
+ Fe T1	106 ± 0.8	1312 ± 280	39
+ Fe T2	127 ± 2	1307 ± 343	36
- Fe T1	89 ± 4	1166 ± 311[b]	40
- Fe T2	10 ± 0.8	279 ± 131[c]	46

[a]90 000 pixels were selected for each analysed field;
[b]Not significantly different from +Fe T1; *p*-value: 0.56 (significance level of 0.05);
[c]Significantly different from +Fe T2; *p*-value: 1.2 10^{-8} (significance level of 0.05).

free in the cytoplasm and were able to fuse, giving rise to very large structures (red arrow, Supplementary fig. S5). Histogram profiles showed a net increase (about 5-fold) in the number of pixels above the background noise between the conditions with and without phosphate (Table 3, Fig. 4., Supplementary fig. S5).

To get more insights into the dynamics of lipid droplets we analysed the time series of each pixel in order to get a map of the transmission, the standard deviation, the cumulative sum (Matalb: cumsum function) and the average frequency. Despite a noticeable difference in signal level (standard deviation and cumulative sum, see below) between the cells grown with and without Pi, we did not observe any significant differences with regard to the central frequencies, which were around 15 ± 5 Hz. We

Table 2. Diameter and dynamic behaviour of droplets in full or phosphate-depleted medium.

	Average droplet diameter (µm ± SD) (number of analysed droplets)	Number of droplets with dynamic behaviour (percentage)
+ Pi: exp1	0.56 ± 0.22 (42)	22 (52%)
− Pi: exp1	0.97 ± 0.33 (58)	55 (94%)
+ Pi: exp2	0.43 ± 0.11 (18)	6 (33%)
− Pi: exp2	0.96 ± 0.32 (26)	21 (80%)
+ Pi: exp3	0.51 ± 0.21 (26)	12 (46%)
− Pi: exp3	0.88 ± 0.22 (86)	61 (71%)

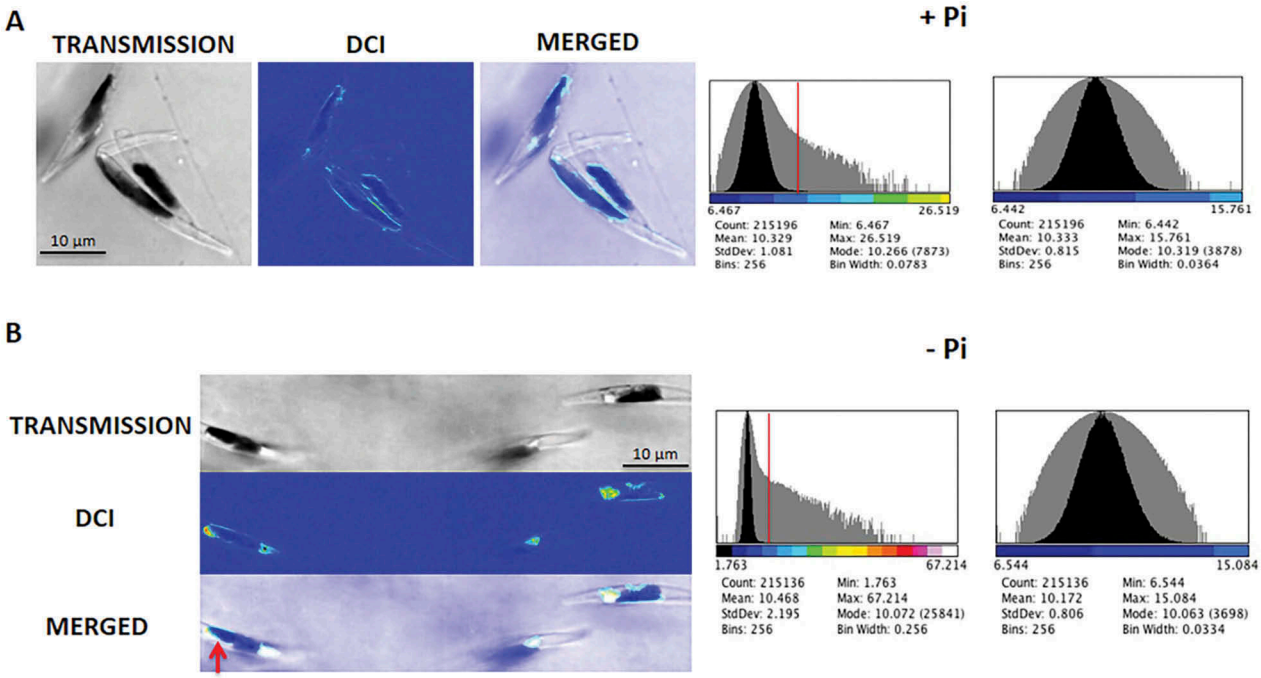

Fig. 4. Increase in lipid droplets size and numbers in *Phaeodactylum tricornutum* cells grown for 8 days in phosphate-depleted medium. From left to right panel (top to bottom) are shown the transmission (single capture from the 100 frames movie), the standard deviation of each pixel of the same field over the 100 frames and the merged image (artificial blue colour). Red arrow indicates lipid droplet in phosphate-depleted medium. Histograms of the standard deviation images using image J (Fiji) were recorded and the number of pixels above noise level were computed (indicated by a red bar on the histogram). Histograms of the same image size without cells were recorded to determine noise levels. Scale bar values were deduced from the format of the image (60 × 60 µm).

Table 3. Comparison of movements of *Phaeodactylum* scatterers, computing their standard deviation or cumulative sum in media with or without phosphate

	Number[a] of dynamic pixels ±SD (method: standard deviation)	Number of dynamic pixels ±SD (method: Cumulative sum)	Ratio Cumulative sum/ Standard deviation
+Pi	586 ± 167	1174 ± 196	2
-Pi	2844 ± 155	3311 ± 236	1.16

[a]Three stacks were analysed in each condition. A total of 33 000 pixels was selected for each analysed field.

observed a 3–5 times increase in the signal amplitude (standard deviation and cumulative sum respectively) in *P. tricornutum* grown without phosphate (Table 3). The analysis of the signal value also pointed out some differences in the signal distribution between standard deviation and cumulative sum computations. The computation of value variation of a pixel, based on the cumulative sum of the signals, highlighted a non-Brownian displacement within the lipid droplets (Table 3). Following the method developed in Scholler (2019) we found that the normalized cumulative sum is about twice that of the normalized standard deviation in culture with phosphate while it is slightly greater (×1.2) in culture without phosphate (Table 3). This result suggests that the random movement of scatterers within the droplets is likely to be associated with a drift that makes it hyper-diffusive, rather than being a pure Brownian motion and could correspond to the flux of lipids and proteins filling lipid bodies (Olzmann & Carvalho, 2019; Nettebrock & Bohnert, 2020).

Discussion

Here, we present a non-invasive (no genetic manipulation) and non-destructive (no fixation step) method, which allows the detection and characterization of internal movements within photosynthetic cells. In particular, through image analysis we show evidence that these dynamic processes are correlated with the functioning of the chloroplasts. This detection was possible by relying on the scattering properties of the cell organelles and of the high frame rate of our camera recordings. We were able to identify and quantify movements within lipid droplets, specific organelles, which accumulate in nutrient-stressed diatoms. In cells deprived of phosphate, in addition to the random movement of little scatterers, which may correspond to the movement of membrane proteins from ER (Jacquier *et al.*, 2011) or storage of misfolded proteins in lipid droplets as suggested by Lupette *et al.* (2019), we described a drift movement of scatterers, which might correspond to molecular fluxes of proteins and/or lipids. The distribution of dynamic pixels which were often observed in an eggcup shape (Supplementary fig. S6) could be in agreement with the ER surrounding lipid droplets (Jacquier *et al.*, 2011) and more precisely in the specific case of diatoms the outermost membrane of the chloroplast (Flori *et al.*, 2016; Jaussaud *et al.*, 2020; Leyland *et al.*, 2020).

Cytoplasmic streaming generated by myosin in the alga *Chara* or in plants has long been known (reviewed by Tominaga & Ito, 2015). Indeed the speed of cytoplasmic streaming generated by *Chara* myosin observed by optical trap nanometry is in the range of 50 µm s^{-1} (Tominaga & Ito, 2015). With DCI we observed live imaging of low speed movements (about 0.1 µm s^{-1}) of undetectable scatterers within *P.tricornutum*organelles, corresponding to their metabolic activity. The DCI method can be extended to any microalgae even though transformation is not available for many of them. For example, we have studied the polar diatom *Fragilariopsis cylindrus* grown under light or in dark, alongside polar, temperate and tropical isolates of the haptophyte genus *Pavlova* grown under multiple environmental temperatures, identifying differences in dynamic cell structure in each case (unpublished data). The method is very sensitive and allows the study of slight changes due to environmental fluctuations such as variation in CO_2 concentration, light quality responses, or nutrient abundance. In addition, most of the image analyses have been run in Fiji (ImageJ), a public domain application (Schindelin *et al.*, 2012).

Cell exploration by microscopic techniques has recently made tremendous progress (Kwon, 2021) however most of these require skill and expensive equipment. Here we used a very simple set up (Thouvenin *et al.*, 2021) to rapidly analyse diatom cells under stress. The DCI method can easily be used as a non-intrusive first step before in depth investigations of intracellular movements via FRAP, single-cell -resolution secondary ion mass spectroscopy (SIMS) or other techniques.

Acknowledgements

We wish to thank our colleagues: Ignacio Izzedine (Institut Langevin) for the use of the fluorescence microscope, Olivier Thouvenin (Institut Langevin) for his help in the dynamic signal analysis, and Benjamin Bailleuil (IBPC) for providing photosystem II inhibitors.

Disclosure statement

No potential conflict of interest was reported by the authors.

Funding

Houda Bey, Claude Boccara: DIM ELICIT (INFLUERE IN VISCERA).Florent Charton: Q-life (Q-life ANR.-17-CONV-0005). Helena Cruz de Carvalho: Agence Nationale de la Recherche (ANR DiaLincs 19-CE43 -0011-01 585). Richard Dorrell: CNRS (CNRS Momentum Fellowship). Chris Bowler: ERC (European Research Council, Diatomic project); Agence Nationale de la Recherche (ANR Browncut

Supplementary material

The following supplementary material is accessible via the Supplementary Content tab on the article's online page at https://doi.org/10.1080/09670262.2022.2081732

Figure S1: Simulation of a pure Brownian motion (blue) and of a biased movement (red) where a drift is added to the Brownian motion. The y-axis of the graph shows the dynamic movement of a particle measured over time (x-axis). For this specific example the standard deviation was found to be 1.16 (Brownian) and 1.37 (Brownian biased) whereas the cumsum (cumulative sum) was found to be 12.30 (Brownian) and 180.64 (Brownian biased), demonstrating a very large enhancement of the signal when a drift is present.

Figure S2: Effect of wavelength illumination on intracellular movements in *Phaeodactylum tricornutum* Cells were successively illuminated with pulsed light from LED^{735}(red), LED^{505} (green) and LED^{455} (blue) and a film (100 or 200 frames) of few seconds recorded. The same field of view in the successive acquisition was selected; upper image: transmission; lower image

standard deviation (scale on bottom left) **(figure S2A).** Histograms of the standard deviation images using image J (Fiji) were recorded and the number of pixels above noise level were computed (indicated by a red bar on the histogram) in **figure S2B.** Histograms of the same image for each wavelength, but without cells, were recorded to determine noise levels. Scale bar value was deduced from the format of the image (60x60 μm)

Figure S3: Co-localisation of dynamic lipid droplets from *Phaeodactylum tricornutum* and labelled endoplasmic reticulum Left panel: light microscopy, central panel: GFP fluorescence (grey scale camera, green coloration), right panel merge of the two upper images. Cytosolic (CYT) expressed GFP accumulates in the entire cell. The signal peptide of BIP protein fused to GFP leads to endoplasmic localization of GFP (ER). The dual topogenic signal of Hsp70 fused to GFP targets GFP to periplastid compartment (PPC). Scale bar value was deduced from the format of the image (60x60 μm).

Figure S4: Dynamic signal in Phaeodactylum is not limited to lipid bodies Upper panel: transmission microscopy, central panel: Standard deviation (grey scale camera, 16 colors), lower panel merge of the two previous images. Scale bar value was deduced from the format of the image (90x90 μm).

Figure S5: Decrease in dynamic signal in *Phaeodactylum tricornutum* grown in iron depleted medium Representative cells grown in medium with iron (+Fe) or depleted of iron (-Fe). From left to right panel is shown the transmission, the standard deviation of each pixel and the merged image (artificial blue colour). T1 and T2 correspond to 8 days and 16 days growth in medium with iron or depleted of iron. Histograms of the standard deviation images using image J (Fiji) were recorded and the number of pixels above noise level were computed (indicated by a red bar on the histogram) in **Table 1.** Histograms of the same image size without cells, were recorded to determine noise levels Scale bar value was deduced from the format of the image (60x60 μm)

Figure S6: Diatoms grown with and without Phosphate: Increase in lipid droplets size and numbers in medium depleted in Phosphate

Author contributions

H. Bey: compared interferometry and fluorescence, discussed the results and commented on the manuscript; **F. Charton**: compared interferometry and fluorescence, cultured P. tricornutum and studied its growth under stress, discussed the results and commented on the manuscript; **H.C. de Carvalho**: contributes to the writing of the manuscript, discussed the results and commented on the manuscript; **S. Liu**: cultured P. tricornutum and studied its growth under stress, discussed the results and commented on the manuscript; **R.G. Dorrell**: built the GFP fusions, contributes to the writing of the manuscript, discussed the results and commented on the manuscript; **C. Bowler**: contributes to the writing of the manuscript, discussed the results and commented on the manuscript; **C. Boccara**: built, characterized the optical setup and analysed the movies and wrote the manuscript, discussed the results and commented on the manuscript; **M. Boccara**: performed and analysed the biological experiments and wrote the manuscript, discussed the results and commented on the manuscript.

References

Abida, H., Dolch, L.J., Mei, C., Villanova, V., Conte, M., Block, M.A., Finazzi, G., Bastien, O., Tirichine, L., Bowler, C., Rebeille, F., Petroutsos, D., Jouhet, J. & Marechal, E. (2015). Membrane glycerolipid remodeling triggered by nitrogen and phosphorus starvation in *Phaeodactylum tricornutum*. *Plant Physiology*, **167**: 118–136.

Alboresi, A., Perin, G., Vitulo, N., Diretto, G., Block, M., Jouhet, J., Meneghesso, A., Valle, G., Giuliano, G., Marechal, E. & Morosinotto, T. (2016). Light remodels lipid biosynthesis in *Nannochloropsis gaditana* by modulating carbon partitioning between organelles. *Plant Physiology*, **171**: 2468–2482.

Alipanah, L., Rohloff, J., Winge, P., Bones, A.M. & Brembu, T. (2015). Whole-cell response to nitrogen deprivation in the diatom *Phaeodactylum tricornutum*. *Journal of Experimental Botany*, **66**: 6281–6296.

Alipanah, L., Winge, P., Rohloff, J., Najafi, J., Brembu, T. & Bones, A.M. (2018). Molecular adaptations to phosphorus deprivation and comparison with nitrogen deprivation responses in the diatom *Phaeodactylum tricornutum*. *PLoS ONE*, **13**: e0193335.

Apelian, C., Harms, F., Thouvenin, O. & Boccara, C. (2016). Dynamic full field optical coherence tomography: subcellular metabolic contrast revealed in tissues by interferometric signals temporal analysis. *Biomedical Optics Express*, **7**: 1511.

Apt, K.E., Zaslavkaia, L., Lippmeier, J.C., Lang, M., Kilian, O., Wetherbee, R., Grossman, A.R. & Kroth, P. G. (2002). *In vivo* characterization of diatom multipartite plastid targeting signals. *Journal of Cell Science*, **115**: 4061–406

Bailleul, B., Cardol, P., Breyton, C. & Finazzi, G. (2011). Electrochromism: a useful probe to study algal photosynthesis. *Photosynthesis Research*, **106**: 179–189. Erratum in: *Photosynthesis Research*, **10**: 151–152.

Bowler, C., Vardi, A. & Allen, A.E. (2010). Oceanographic and biogeochemical insights from diatom genomes. *Annual Review of Marine Science*, **2**: 333–365.

Cavalier-Smith, T. (1999). Principles of protein and lipid targeting in secondary symbiogenesis: euglenoid, dinoflagellate, and sporozoan plastid origins and the eukaryote family tree. *Journal of Eukaryotic Microbiology*, **46**: 347–366.

Cruz de Carvalho, H., Sun, H.X., Bowler, C. & Chua N.H. (2016). Noncoding and coding transcriptome responses of a marine diatom to phosphate fluctuations. *New Phytologist*, **210**: 497–510.

De Martino, A., Meichenin, A., Shi, J., Pan, K. & Bowler C. (2007). Genetic and phenotypic characterization of *Phaeodactylum tricornutum* (Bacillariophyceae) accessions. *Journal of Phycology*, **43**: 992–1009.

Domingues, N., Matos, A.R., Marques da Silva, J. & Cartaxana, P. (2012). Response of the diatom *Phaeodactylum tricornutum* to photooxidative stress resulting from high light exposure. *PLoS ONE*, **7**: e38162.

Falciatore, A, Casotti, R., Leblanc, C., Abrescia, C. & Bowler, C. (1999). Transformation of nonselectable reporter genes in marine diatoms. *Marine Biotechnology (NY)*, **1**: 239–251.

Falciatore, A., Jaubert, M., Bouly, J-P, Bailleul, B. & Mock, T. (2020). Diatom molecular research comes of age: model species for studying phytoplankton biology and diversity. *The Plant Cell*, **32**: 547–572.

Flori, S., Jouneau, P.H., Finazzi, G., Maréchal, E. & Falconet D. (2016). Ultrastructure of the periplastidial compartment of the diatom *Phaeodactylum tricornutum*. *Protist*, **167**: 254–267.

Gao, X., Bowler, C. & Kazamia, E. (2021). Iron metabolism strategies in diatoms. *Journal of Experimental Botany*, **72**: 2165–2180.

Goss, R., Wilhelm, C. & Jakob, T. (2020). Photosynthesis in diatoms. In *Handbook of Algal Science, Technology and Medicine* (Konur, O., editor), 217–229. Academic Press, London.

Gould, S.B., Sommer M.S., Kroth P.G., Gile G.H., Keeling P.J. & Maier U.G. (2006). Nucleus-to-nucleus gene transfer and protein retargeting into a remnant cytoplasm of cryptophytes and diatoms. *Molecular Biology and Evol*ution, **23**: 2413–2422.

Jacquier, N., Choudhary, V., Mari, M., Toulmay, A., Reggiori, F. & Schneiter, R. (2011). Lipid droplets are functionally connected to the endoplasmic reticulum in *Saccharomyces cerevisiae*. *Journal of Cell Science*, **124**: 2424–2437.

Jaussaud, A., Lupette, J., Salvaing, J., Jouhet, J., Bastien, O., Gromova, M. & Maréchal E. (2020). Stepwise biogenesis of subpopulations of lipid droplets in nitrogen starved *Phaeodactylum tricornutum* cells. *Frontiers in Plant Sci*ence, **11**: 48.

Kazamia, E., Sutak, R., Paz-Yepes, J., Dorrell, R.G., Rocha Jimenez Vieira, F., Mach, J., Morrissey, J., Leon, S., Lam, F., Pelletier, E., Camadro, J-M., Bowler, C. & Lesuisse, E. (2018). Endocytosis-mediated siderophore uptake as a strategy for Fe acquisition in diatoms. Science Advances, **4**: eaar4536.

Kolber, Z., Barber, R., Coale, K. et al. (1994). Iron limitation of phytoplankton photosynthesis in the equatorial Pacific Ocean. *Nature*, **371**: 145–149.

Kwon, D. (2021). Proteins in their natural habitats *Nature*, **598**: 558–560

Leyland, B., Boussiba, S. & Khozin-Goldberg, I. (2020). A review of diatom lipid droplets. *Biology* (Basel), **9**: 38.

Liang, Y., Koester, J.A., Liefer, J.D, Irwin, A.J. & Finkel, Z. V. (2019). Molecular mechanisms of temperature acclimation and adaptation in marine diatoms. *ISME Journal*, **13**: 2415–2425.

Liu, X., Hempel, F., Stork, S., Bolte, K., Moog, D., Heimerl, T., Maier, U.G. & Zauner, S. (2016). Addressing various compartments of the diatom model organism *Phaeodactylum tricornutum* via sub-cellular marker protein. *Algal Research*, **20**: 249–257.

Lupette, J., Jaussaud, A., Seddiki, K., Morabito, C., Brugière, S., et al. (2019). The architecture of lipid droplets in the diatom *Phaeodactylum tricornutum*. *Algal Research – Biomass, Biofuels and Bioproducts*, **38**: 101415.

Nettebrock, N.T. & Bohnert, M. (2020). Born this way – biogenesis of lipid droplets from specialized ER subdomains. *BBA – Molecular and Cell Biology of Lipids*, **1865**: 158448.

Olzmann, J.A. & Carvalho, P. (2019). Dynamics and functions of lipid droplets. *Nature Review of Molecular Cell Biology*, **20**: 137–155.

Pierella Karlusich, J.J., Ibarbalz, F.M. & Bowler, C. (2020). Phytoplankton in the Tara Ocean. *Annual Review of Marine Science*, **12**: 233–265.

Prins, A., Deleris, P., Hubas, C. & Jesus, B. (2020). Effect of light intensity and light quality on diatom behavioral and physiological photoprotection. *Frontiers in Marine Science*, **7**: 203.

Roncel, M., González-Rodríguez, A.A., Naranjo, B., Bernal-Bayard, P., Lindahl, A.M., Hervás, M., Navarro, J.A. & Ortega, J.M. (2016). Iron deficiency induces a partial inhibition of the photosynthetic electron transport and a high sensitivity to light in the diatom *Phaeodactylum tricornutum*. *Frontiers in Plant Science*, **7**: 1050.

Saunter, C.D., Perng, M., Love, G. & Quinlan, R. (2009). Stochastically determined directed movement explains the dominant small-scale mitochondrial movements within non-neuronal tissue culture cells. *FEBS Letters*, **583**: 1267–1273.

Scholler, J. (2019). Motion artifact removal and signal enhancement to achieve in vivo dynamic full field OCT. *Optics Express*, **27**: 19562–19572.

Scholler, J., Mazlin, V., Thouvenin, O., Groux, K., Xiao, P., Sahel, J.A., Fink, M., Boccara, C. & Grieve, K. (2019). Probing dynamic processes in the eye at multiple spatial and temporal scales with multimodal full field OCT. *Biomedical Optics Express*, **10**: 731–746.

Schindelin, J., Arganda-Carreras, I., Frise, E., et al. (2012). Fiji: an open-source platform for biological-image analysis. *Nature Methods*, **9**: 676–682.

Thouvenin, O., Boccara, C., Fink, M., Sahel, J.A., Paques, M. & Grieve, K. (2017a). Cell motility as contrast agent in retinal explant imaging with full-field optical coherence tomography. *Investigative Ophthalmology & Visual Science*, **58**: 4605.

Thouvenin, O., Fink, M. & Boccara, C. (2017b). Dynamic multimodal full-field optical coherence tomography and fluorescence structured illumination microscopy. *Journal of Biomedical Optics*, **22**(**2**): 026004.

Thouvenin, O., Alhaddad, S., Mazlin, V., Boccara, M., & Boccara, C. (2021). Label free optical transmission tomography for biosystems: Intracellular structures and dynamics. *arXiv*, 3991089.

Tominaga, M. & Ito, K. (2015). The molecular mechanism and physiological role of cytoplasmic streaming. *Current Opinion in Plant Biology*, **27**: 104–110.

Ustick, L.J., Larkin, A.A., Garcia, C.A., Garcia, N.S., Brock, M. L., Lee, J.A., Wiseman, N.A., Moore, J.K. & Martiny, A.C. (2021). Metagenomic analysis reveals global-scale patterns of ocean nutrient limitation. *Science*, **372**: 287–291.

Yao, S., Brandt, A., Egsgaard, H. and Gjermansen, C. (2012). Neutral lipid accumulation at elevated temperature in conditional mutants of two microalgae species. *Plant Physiology and Biochemistry*, **61**: 71–79.